Theoretical calculation of the wave-vector- and frequency-dependent dielectric function of $YBa_2Cu_3O_7$

H. Chen, J. Callaway, and N. E. Brener

Department of Physics and Astronomy, Louisiana State University, Baton Rouge, Louisiana 70803-4001

Z. Zou

Department of Physics, University of Colorado, Boulder, Colorado 80309-0390

Real and imaginary parts of the dielectric function $\epsilon(\omega,\mathbf{q})$ of $YBa_2Cu_3O_7$ are calculated in the random-phase approximation, based on a parametrized tight-binding band structure. Only the contribution to the dielectric function from electronic interband transitions is considered. Prominent optical absorption peaks are found at 3.0, 2.3, and below 0.6 eV. For energy in the range 0.2–1.5 eV, we find that ϵ_1 is negative in a very large region inside the q_x,q_y plane. Detailed studies on these low-energy absorption peaks reveal that they are mainly associated with the interband charge excitations involving orbitals within the Cu-O plane. For optical properties ($q=0$), our results are compared with experimental data and previously reported theoretical calculations. There is a reasonably good agreement.

I. INTRODUCTION

We present in this paper a theoretical investigation of the dielectric function of $YBa_2Cu_3O_7$ as a function of both the frequency (ω) and the wave vector ($\mathbf{q}$). When a weak external potential is applied to a solid, the electrons readjust their distributions, thus giving rise to a screening potential. This response is described by the dielectric function. The dielectric function is needed in the study of, e.g., optical properties, electron energy loss, electron-phonon interactions, and transport phenomena. It may also be of particular importance in regard to high-T_c superconducting materials. The dielectric function can be used directly to investigate possible pairings mediated by electronic charge excitations (generally termed excitons[1]), and it can be used in a calculation of the transition temperature T_c. The effective interelectron interaction is reasonably approximated by $4\pi e^2/q^2\epsilon(\omega,\mathbf{q})$. It is clear that in order for pairings to occur, $\epsilon(\omega,\mathbf{q})$ has to be negative in certain regions of the $\omega,\mathbf{q}$ space. In a simple model, the effective interelectron interaction is averaged over the wave vector $\mathbf{q}$ as in the case of the BCS theory. In this case, the transition temperature is directly related to the range of frequencies over which the effective interaction is attractive.[1]

A realistic evaluation of the dielectric function requires a reliable set of energy bands and wave functions. The work presented here is based on an accurate tight-binding parametrization[2] of the first-principles, linearized-augmented-plane-wave (LAPW) band structure[3] for $YBa_2Cu_3O_7$. The adequacy of band calculations as a basis for the description of the electronic structure of high-T_c superconductors in their normal state is a matter of serious concern and has been the subject of much debate. However, as a result of improvements in the experimental techniques and better sample preparation, there

now exists a growing body of evidence indicating that many of the electronic properties predicted by band-structure calculations are in good agreement with experiments, especially for $YBa_2Cu_3O_7$ and the Bi-Sr-Ca-Cu-O compound. By effectively controlling the oxygen loss and through other technical improvements, experimentalists can now get a valence-band photoemission spectrum that is in agreement with the theoretical results within 0.5 eV with respect to locations of the peaks, while in the earlier works, the discrepancy is as large as 2 eV.[4] At low frequencies, the dielectric function is very sensitive to the shape of the Fermi surface. Results of the positron-annihilation experiment are in quite good accordance with the Fermi surfaces predicted by band-structure calculations.[5] For $YBa_2Cu_3O_7$ and the Bi-Cu-O compound, photoemission experiments have confirmed the shape of the Fermi surface as predicted by the theory in several directions.[6,7]

The most important issue for $YBa_2Cu_3O_7$ is, of course, to understand the cause (or causes) of superconductivity at 90 K. Many of the current theoretical efforts are focused on effects of spin fluctuations.[8] Models associated with charge fluctuations have also been proposed.[9] The knowledge of the dielectric function is uniquely useful to further elucidate charge fluctuations. In the present work, we demonstrate that below 0.5 eV the dielectric function for $YBa_2Cu_3O_7$ is very rich in structure. We find that within the q_x,q_y plane, due to strong interband transitions, ϵ_1 is negative in a large region of the $\omega,\mathbf{q}$ space. The effect of these interband excitations on superconductivity is presently being studied. In this work, we will explore the $\omega,\mathbf{q}$ dependence of the dielectric function.

Previously published theoretical studies of the dielectric function of $YBa_2Cu_3O_7$ have only considered the $q=0$ limit which describes optical properties. The work

reported by Zhao et al.[10] was based on a band structure calculated by the orthogonalized-linear-combination-of-atomic-orbitals method, and emphasized gross features at relatively high energies (up to 8 eV). The work of Chui, Kasowski, and Hsu[11] concentrated more on structures of the optical conductivity in the low-energy range 0–1 eV, which was computed from first-principles bands that were obtained by the pseudofunction method. These papers concluded that interband transitions should dominate the whole frequency range above the far-infrared region. In this paper, we will present results of the dielectric function calculated for both $q = 0$ and $q \neq 0$ cases. In the case of $q = 0$, our results agree well with previous cal-

culations. And in this case, we will also make comparisons with the experimental measurements recently carried out by Schlesinger et al.[12] Electron energy-loss experiments,[13–15] which involve $\epsilon(\omega, q)$ for nonzero q have been performed over a wide range of energies (0–40 eV) but the structure in the loss spectrum in the energy range of primary interest here has not been resolved.

II. METHOD

Our calculation is based on the formulation of the random-phase approximation (RPA). The dielectric function is given by

$$\epsilon(\omega, \mathbf{q}) = 1 - \frac{4\pi e^2}{q^2} \frac{2}{N\Omega} \sum_{n,l,\mathbf{k}} f_n(\mathbf{k})[1 - f_l(\mathbf{k}-\mathbf{q})] \langle n, \mathbf{k} | \exp(i\mathbf{q} \cdot \mathbf{r}) | l, \mathbf{k}-\mathbf{q} \rangle \langle l, \mathbf{k}-\mathbf{q} | \exp(-i\mathbf{q} \cdot \mathbf{r}) | n, \mathbf{k} \rangle$$

$$\times \left[\frac{1}{\omega + E_n(\mathbf{k}) - E_l(\mathbf{k}-\mathbf{q}) + i\delta} - \frac{1}{\omega - E_n(\mathbf{k}) + E_l(\mathbf{k}-\mathbf{q}) + i\delta} \right] , \qquad (1)$$

where Ω is the volume of the unit cell, N is the number of unit cells inside a macroscopic volume, $E_n(\mathbf{k})$ and $|n, \mathbf{k}\rangle$ are the energy bands and corresponding wave functions, and f is the Fermi function. In Eq. (1), the summation on the band index n does not include the index for spin. The real and imaginary parts of the dielectric function can be separated by the identity $1/(x + i\delta) = P(1/x) - i\pi\delta(x)$, where $P(1/x)$ indicates the principal part. In a crystal, the dielectric function is actually[16] a matrix $\epsilon_{s,t}$, with indices corresponding to the reciprocal lattice vectors $\mathbf{K}_s$ and $\mathbf{K}_t$. In the present work, this lattice effect is

ignored and we only consider the element $\epsilon_{0,0}$.

We evaluate Eq. (1) by using realistic band structure and wave functions obtained from a tight-binding fit by DeWeert, Papaconstantopoulos, and Pickett.[2] The quality of the fit appears to be very good for bands around the Fermi level. This band structure is shown in Fig. 1. Major pieces of the Fermi surface are well reproduced by the fit except for the small hole pocket around the S point. It is clearly seen from Fig. 3 of Ref. 3 that this pocket is due to a band associated with the Cu-O chains. Several bands just below this feature are also associated with the chains.
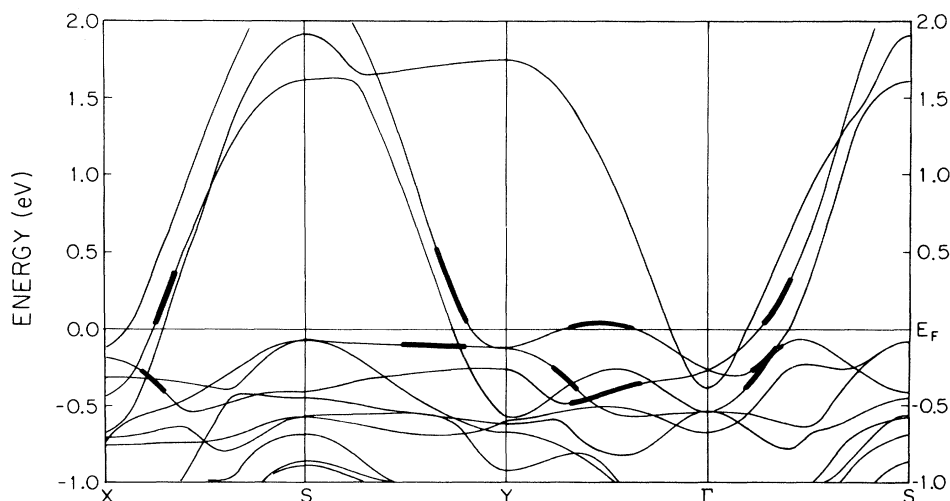

FIG. 1. Band structure of $YBa_2Cu_3O_7$ calculated by a parametrized 36×36 Hamiltonian. Emphasized portions of the band structure make important contributions to the dielectric function and optical conductivity for energies less than 1 eV.

This error in the band fit will thus not affect the important low-energy features in the dielectric function which are connected with the excitations within Cu-O planes. It is also clear[3] that bands around the Fermi level (within 1 or 2 eV) are predominantly composed of Cu d and O p orbitals. In the current calculation, we therefore neglect all orbitals associated with Y and Ba and use the band structure calculated using a reduced Hamiltonian (36×36). The reduction is furnished by Papaconstanto-poulos[17] based on their original fit[2] using a Hamiltonian of dimension 82×82. This reduction does not cause further significant changes of bands around the Fermi level.

To calculate the matrix elements in Eq. (1), we use the following tight-binding formula:

$$\langle n, \mathbf{k} | \exp(i\mathbf{q} \cdot \mathbf{r}) | l, \mathbf{k} - \mathbf{q} \rangle = \sum_{\mu} \exp[i(\mathbf{k} - \mathbf{q}) \cdot \mathbf{R}_{\mu}] \sum_{i,j} C_{in}^{*}(\mathbf{k}) C_{jl}(\mathbf{k} - \mathbf{q}) \int U_{i}^{*}(\mathbf{r}) \exp(i\mathbf{q} \cdot \mathbf{r}) U_{j}(\mathbf{r} - \mathbf{R}_{\mu}) d\mathbf{r} \ . \qquad (2)$$

$C_{in}(\mathbf{k})$ is a normalized eigenvector component determined by diagonalization of the tight-binding Hamiltonian. U_{i} is the ith orbital basis function. Some choice of wave functions has to be made in order to enable an evaluation of matrix elements. It is assumed in this approximate treatment that the functions used implicitly in fitting the band structure actually are suitably chosen atomic wave functions. In this work, we have used a Gaussian atomic basis[18] so that integrals in Eq. (2) can be evaluated analytically. Detailed expressions are given in the Appendix.

The $\mathbf{k}$ summation of Eq. (1) can be converted into a Brillouin zone (BZ) integral: $\sum_{\mathbf{k}} = N\Omega/(2\pi)^3 \int_{BZ}$. The integrations are carried out numerically by the linear tetrahedron method in the whole BZ. For ϵ_1, the principal-value integrals are evaluated following the procedure given by Rath and Freeman.[19] The integration for ϵ_2 is similar to the standard computation of the density of states.[20] The total number of grid points used inside the total zone is 2023. The numerical integrations were tested by comparing with the exact values of ϵ_1 for the free-electron model.[21] The uncertainties are around 1–3 %. A similar magnitude of uncertainty is also found when we change the total number of integration points. Since ϵ_1 and ϵ_2 are both calculated directly from Eq. (1), it is desirable to see how well they obey the Kramers-Kronig relations.[22] Such a check is shown in Table I, in which we compare the ϵ_1 calculated from direct BZ integration with that obtained through the Kramers-Kronig (KK) relation,

$$\epsilon_1(\omega) = 1 + \frac{2}{\pi} P \int_0^{\infty} \frac{\mu \epsilon_2(\mu)}{\mu^2 - \omega^2} d\mu \ . \qquad (3)$$

Good agreement exists, indicating a high degree of accuracy of our numerical computations. In Table I we also list values of ϵ_1 calculated using the Slater-type atomic orbital basis[23] involving on-site approximations.[24] It is seen that there is also a good agreement between the results calculated using a different orbital basis. The comparison is made at $\mathbf{q} = (0, 0, 0.5)$. Throughout this paper, we will use a reduced unit for the momentum vector $\mathbf{q}$ in $(\pi/a, \pi/b, \pi/c)$. We take the lattice constants[2] $a = 7.224\,95$ a.u., $b = 1.016\,55a$ and $c = 3.055\,99a$.

The RPA formula is well known to produce undesirable results at large $\mathbf{q}$—corresponding to the interelectron distance less than the Thomas-Fermi screening length: $q^{-1} < \kappa^{-1} [\kappa^2 = 4\pi e^2 D(E_F)]$. The calculated density of states per unit volume at the Fermi level $[D(E_F)]$ for $YBa_2Cu_3O_7$ is[2,3] around $0.0512/Ry$ a.u.[3] ($\kappa = 1.134$ a.u.). We can study the correction to the RPA by the Hubbard formula,[25]

$$\epsilon(\omega, \mathbf{q}) = 1 - \frac{V_c(q) \chi(\omega, \mathbf{q})}{1 - G(q) V_c(q) \chi(\omega, \mathbf{q})} \ , \qquad (4)$$

where $V_c(q) = 4\pi e^2/q^2$, $\chi(\omega, \mathbf{q})$ is the susceptibility, and $G(q) = 0.5q^2/(q^2 + \kappa^2)$. Evaluation of Eq. (4) indicates that for the wave vectors we're interested in this paper ($q < 1$ a.u.), the Hubbard correction is very small (less than a few percent).

TABLE I. Results for ϵ_1 obtained by direct calculations are compared with those obtained from ϵ_2 by a Kramers-Kronig transformation of Eq. (3) at $\mathbf{q} = (0, 0, 0.5)$. The calculations of columns 1 and 2 were made with Gaussian wave functions. Column 3 contains the results when a basis of Slater orbitals are used (additional approximations are necessary in this case).

ω (eV)	Direct calculation (Gaussian)	KK	Direct calculation (Slater)
0.105	86.599	83.464	84.068
0.205	65.168	62.790	63.225
0.305	24.475	24.160	23.040
0.405	22.163	22.575	20.503
0.505	6.493	8.086	5.159
0.605	12.254	12.509	10.857
0.705	13.047	13.027	11.460
0.805	10.256	10.775	8.599
0.905	13.951	13.961	12.338
1.005	16.530	16.408	14.765
1.105	18.311	18.017	16.417
1.205	16.103	16.077	14.172
1.305	14.143	14.161	12.126
1.405	13.284	13.266	11.195
1.505	12.642	12.611	10.622
1.605	12.003	11.978	10.225
1.705	12.736	12.568	10.926
1.805	11.391	11.377	9.801
1.905	10.041	10.059	8.629
2.005	11.096	10.745	9.495
2.205	10.806	9.478	8.716
2.405	−16.355	−16.381	−15.630
2.605	−12.378	−12.248	−13.009
2.805	−7.429	−7.462	−8.240
3.005	−9.319	−9.828	−9.175

III. RESULTS AND DISCUSSION

A. $q \neq 0$ case

We begin with a general overview of the dielectric function in the energy range 0–2 eV. Figures 2(a)–2(d) show contour plots of ϵ_1 along four symmetry lines: (a) for (1,0,0); (b) for (1,1,0); (c) for (0,1,0), and (d) for (0,0,1), where heavy lines represent contours of positive values, and values of adjacent contours differ by a factor of 2. From Figs. 2(a)–2(c), it is seen that ϵ_1 becomes negative in a substantially large region of the $\mathbf{q}, \omega$ space roughly defined by $0 < q_{x,y} < 0.5(\pi/a)$; $0.2 < \omega < 1.5$ eV. Figure 2(a) looks fairly similar to Fig. 2(c), but subsequent studies presented below show that the dielectric function in the x and y directions are rather strongly anisotropic. There are structures in Fig. 2(d) at 0.5 and 1.2 eV. They appear to be dispersionless as q is increased along the (0,0,1) direction, which is expected from the quasi-two-dimensional nature of the electronic structure. In Fig. 2(d), there is also a small region in which ϵ_1 is negative at $q > 0.8(\pi/c)$ and $0.4 < \omega < 0.6$ eV. From these contour
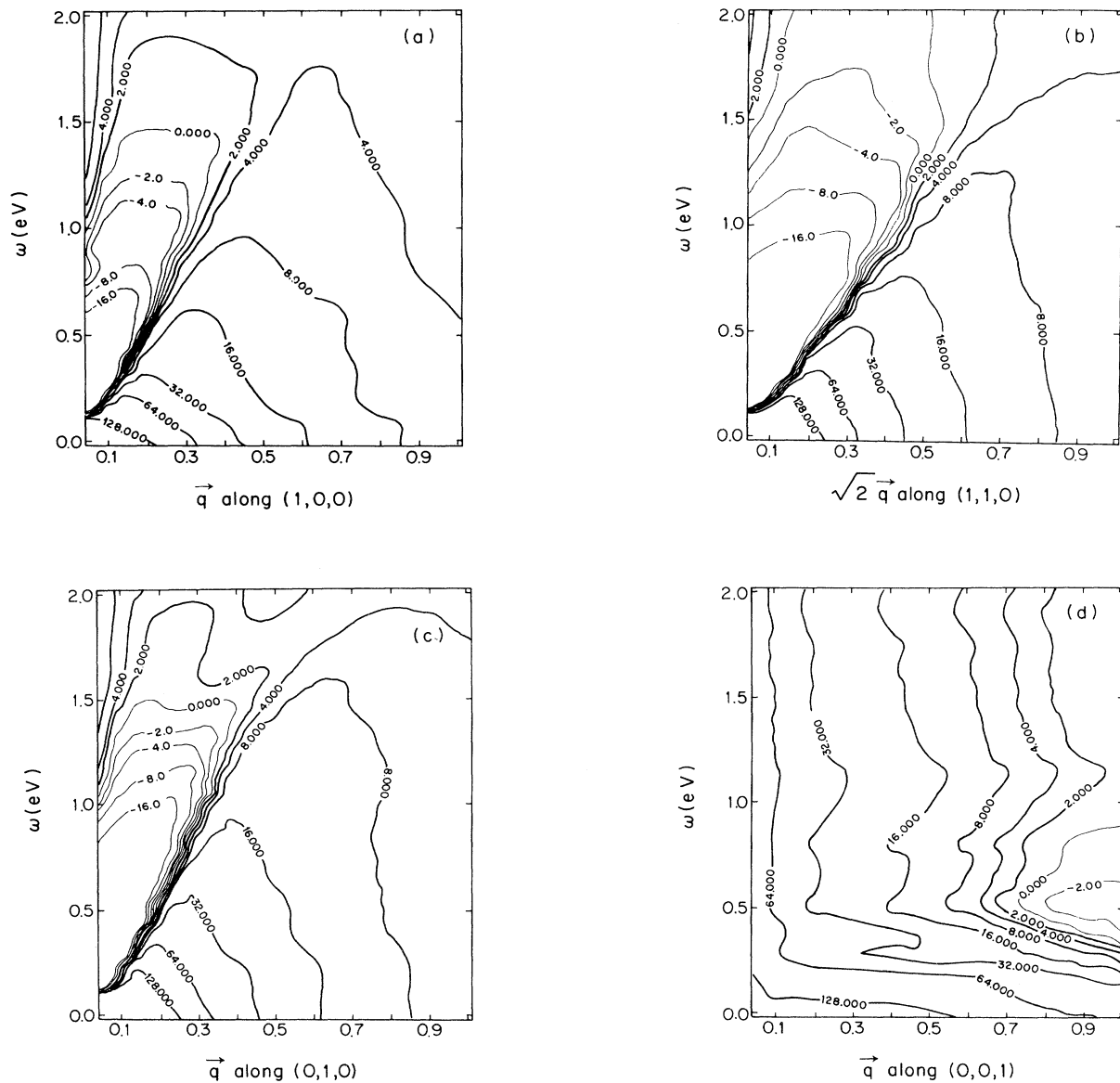

FIG. 2. Contour plots of ϵ_1 in four symmetry directions: (a) (1,0,0), (b) (1,1,0), (c) (0,1,0), and (d) (0,0,1). Values of adjacent contours differ by a factor of 2. Heavy lines indicate the positive value.
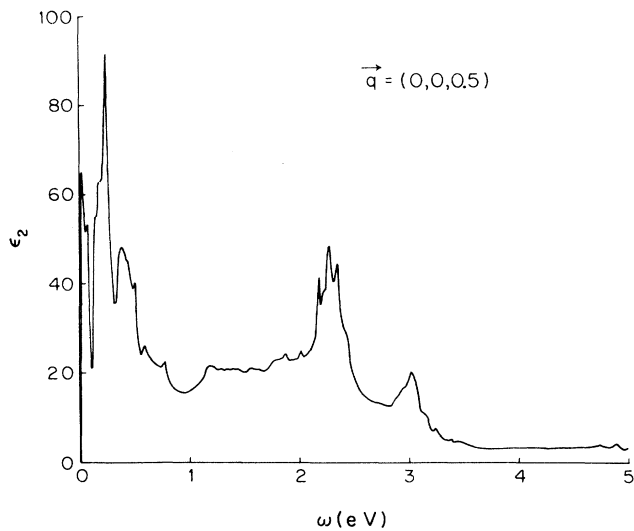
FIG. 3. Imaginary part of the dielectric function for $q = (0,0,0.5)$.

FIG. 5. Imaginary part of the dielectric function for three different q values in the q_x, q_y plane: solid line, (0.1,0.1,0); short-dashed line (0.15,0,0); long-dashed line, (0,0.15,0).

plots, it may seem that ϵ_1 decays more slowly in the z direction. This actually is not the case because the wave vector q is expressed in terms of the reduced units $(\pi/a, \pi/b, \pi/c)$.

Figure 3 shows the imaginary part of the dielectric function for $q_z = 0.5(\pi/c)$ in a broader range of energy. It is seen here that in addition to those strong low-energy peaks below 0.5 eV, there are two additional peaks centered at 2.3 and 3.0 eV. The absorption peak at 2.3 eV is quite strong. Experimentally, a 2.5-eV electronic transition was claimed to be seen[26] in the optical conductivity of ceramic $YBa_2Cu_3O_7$, but detailed information was not provided in that report, and was not reported in other in-

vestigations in the same energy range. The cutoff in band fitting limits our calculation to a range of energies of 5 eV and below. The low-energy structures will be studied in detail below and for the $q = 0$ case in the next subsection.

The low-energy features deserve a closer look because of possible connections between the high-T_c superconductivity and elementary excitations in this energy range.[9] Figures 4, 5, and 6 show ϵ_1, ϵ_2, and the electron energy-loss function, $-\mathrm{Im}(\epsilon^{-1})$, in the energy range 0–3 eV for three different q values: (0.15,0,0), (0,0.15,0), (0.1,0.1,0). The strongly anisotropic nature of the dielec-
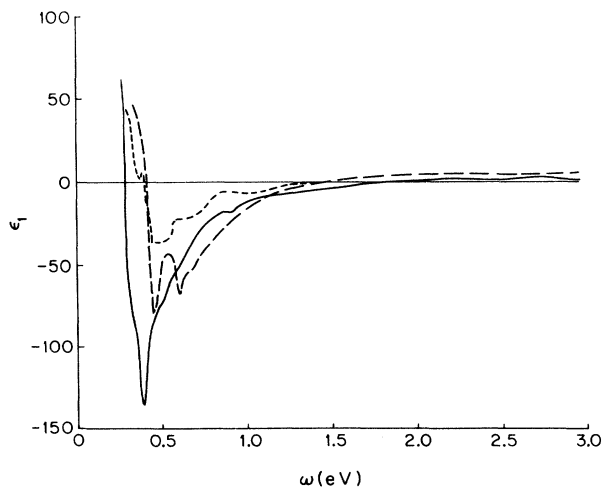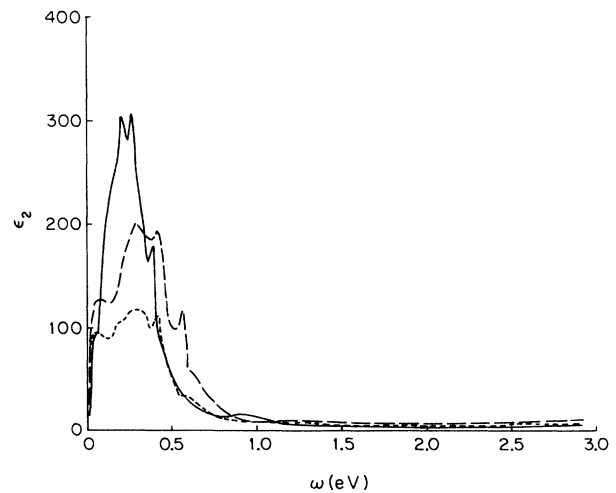

FIG. 4. Real part of the dielectric function for three different q values in the q_x, q_y plane: solid line, $q = (0.1,0.1,0)$; short-dashed line, $q = (0.15,0,0)$; long-dashed line, $q = (0,0.15,0)$.
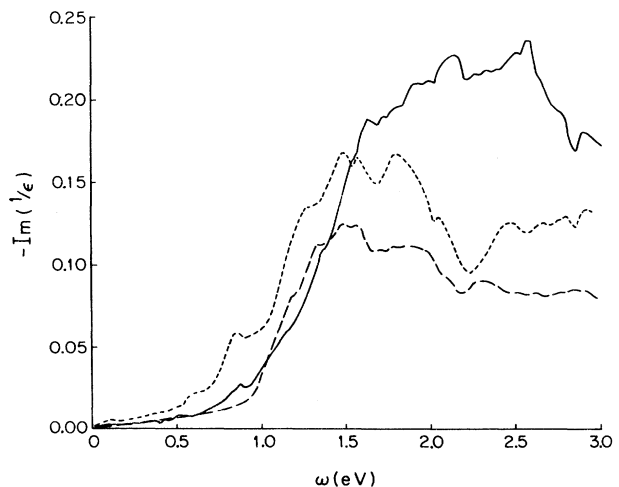

FIG. 6. The electron energy-loss function for three different q values in the q_x, q_y plane: solid line, (0.1,0.1,0); short-dashed line (0.15,0,0); long-dashed line, (0,0.15,0).
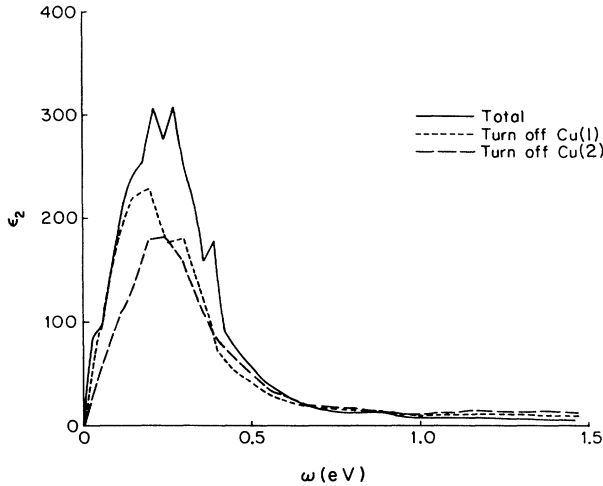
FIG. 7. Imaginary part of the dielectric function for $q=(0.1,0.1,0)$. The effect of turning off the contribution from orbitals centered on different copper sites is shown: solid line, total ϵ_2; short-dashed line, turning off Cu(1); long-dashed line, turning off Cu(2).

We have investigated the origin of these interband transitions. To do this, we take advantage of the tight-binding formulation of the matrix elements in Eq. (2) and arbitrarily let the matrix elements associated with one, or a set of, specific orbitals to be zero. This effectively "turns off" the contribution to the dielectric function from those orbitals. Several curves corresponding to turning off orbitals centered on different atoms are given in Figs. 7 and 8. From these two figures, it can be observed that lower-energy transitions (<0.25 eV) are more strongly affected by turning off orbitals centered at Cu(2) or O(2), indicating the importance of the Cu-O plane. Turning off O(1) (the chain oxygen) gives the smallest effect, but it is evident from Figs. 7 and 8 that Cu(1) also contributes to the low-energy excitations substantially. We can also turn off orbitals associated with a specific atomic symmetry. We find that oxygen p_x and p_y orbitals affect the results most. In addition to the above studies on the atomic orbital effect, we have also compared the interband-transition matrix elements between bands immediately above and below the Fermi level. In Fig. 1, the emphasized bands give relatively larger values of interband transition by about a factor of 10 in comparison with those not emphasized.

tric function is quite evident even within the q_x,q_y plane. From these figures, it is seen that the strength of interband transition is the weakest in the q_x direction and the strongest in the (1,1,0) direction. Comparison between Figs. 5 and 6 indicates that while the greatest strength of interband transitions is concentrated at lower energies (<0.5 eV), the electron energy-loss function starts to rise after 1.0 eV, implying a relatively higher plasmon frequency (1.5–2.5 eV).
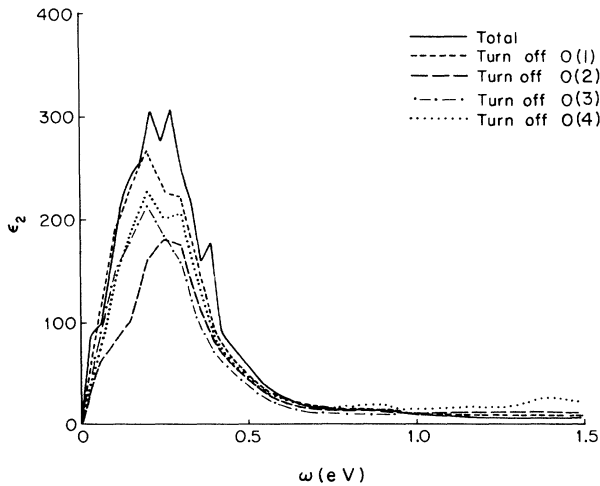
B. $q=0$ case

We now present the results of our calculation in the case of $q=0$, corresponding to the optical excitations. We evaluated ϵ_1 and ϵ_2 after taking the $q=0$ limit in Eq. (1). The dielectric function is a tensor. In Fig. 9, we present calculated ϵ_1^{xx} and ϵ_1^{yy} in comparison with the experimental data by Schlesinger et al.[12] The experiment measures the $(a$-$b)$ plane reflectivity directly. The Kramers-Kronig relations are used to convert this data into ϵ_1 and ϵ_2. There is a rather good agreement between theory and experiment for energy greater than 0.5 eV.
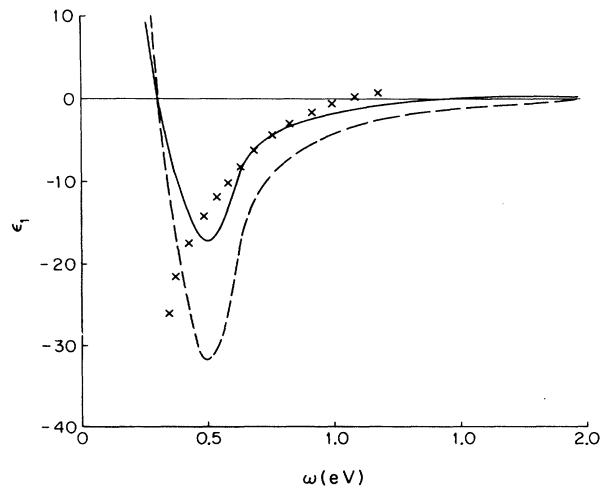

FIG. 8. Imaginary part of the dielectric function for $q=(0.1,0.1,0)$. The effect of turning off the contribution from orbitals centered on different oxygen sites is shown: solid line, total ϵ_2; short-dashed line, turning off O(1); long-dashed line, turning off O(2); dotted and long-dashed line, turning off O(3); dotted line, turning off O(4).

FIG. 9. Real part of the dielectric function for $q=0$: solid line, ϵ_1^{xx}; long-dashed line, ϵ_1^{yy}. Crosses are experimental data of Ref. 12.

The calculated dielectric functions above 0.5 eV are slightly lower than the measured values. For energies less than 0.5 eV, experiment data and theoretical curves diverge. The calculated ϵ_1 begin to rise while the experimental data continue to decrease.

Our present calculation includes only interband contributions to the dielectric function and does not incorporate the effect of relaxation. We have ignored the contributions of lattice vibrations which should strongly influence $\epsilon_2(\omega)$ for energies less than a few hundred wave numbers ($\omega_{ph} < 0.1$ eV). Other sources of relaxation may also be present involving impurities, electron-electron scattering, and possibly magnetic excitations. Due to the Kramers-Kronig relation, a change in ϵ_2 at low frequencies will affect the shape of $\epsilon_1(\omega)$ in a wide range of frequencies. In particular, as can be easily noted from Eq. (3), an increase of ϵ_2 below some ω_0 causes the real part of the dielectric function to decrease in proportion to $1/(\omega^2 - \omega_0^2)$ for ω larger than ω_0. Experimentally,[12] it is found that the relaxation rate τ^{-1} is rather large for YBa$_2$Cu$_3$O$_7$ ($\tau^{-1} \sim 0.1$ eV at $\omega = 0$). And $\tau^{-1}(\omega)$ increases almost linearly with ω. A frequency-dependent $\tau^{-1}(\omega)$ is difficult to incorporate into the calculation since the Kramers-Kronig relations may no longer apply. The most obvious effect of a large relaxation rate is to obliterate sharp structures. Additionally, in the present calculation, we have not considered the singularity of ϵ_2 at $\omega = 0$ corresponding to a finite dc conductivity. This contribution to conductivity is usually added to the interband term phenomenologically by including a Drude term which is centered at $\omega = 0$ with a width determined by the relaxation rate (~ 0.1 eV). Apparently, the inclusion of such a term will also improve the agreement between theory and experiment in a similar way as the inclusion of a phonon term does.

Instead of showing ϵ_2, we present in Fig. 10 the elements of the interband optical conductivity tensor, $\sigma = (\omega/4\pi)\epsilon_2$, σ^{xx}, σ^{yy}, and σ^{zz}. There is a large conductivity peak in the xx and yy components for ω from 0.2 to 0.6 eV. The size of the yy component of conductivity is nearly twice as large as that of the xx component, indicating that there is a substantial contribution to the optical conductivity from Cu-O chains. The zz component is drastically different from those in the xx and yy components. The zz component peaks at a lower energy: 0.1 eV, and it is the weakest of all three. Both the position and the averaged conductivity peak strength of 1900 $(\Omega\,cm)^{-1}$ are in excellent agreement with previously reported theoretical calculations of Chui, Kasowski, and Hsu.[11] However, the experimental situation with regard to this low-energy conductivity peak is unclear at the present stage. An earlier experiment[26] on the ceramic samples showed a conductivity peak at 0.4 eV with a strength of 1200 $(\Omega\,cm)^{-1}$, but other experiments[12,27] have not been able to show such a peak clearly.
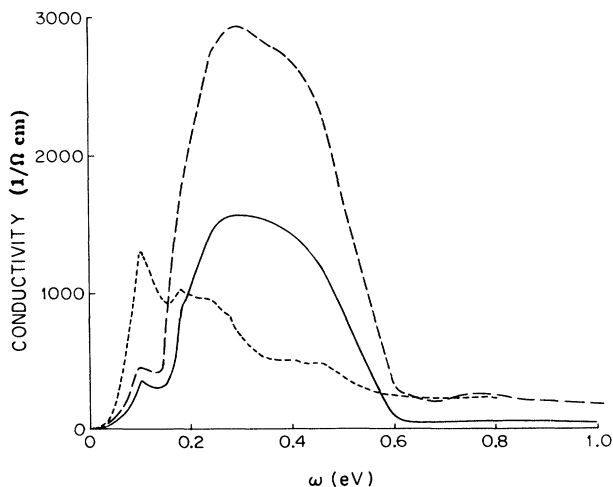
The existence of low-energy structure in the optical conductivity is an inevitable consequence of the complex band structure of Fig. 1. Unfortunately, experiments cannot isolate the interband contribution from the measured conductivity uniquely. In Ref. 12, it is demonstrated that the infrared conductivity does not diminish with frequency as rapidly as $1/\omega^2$, which is expected from the Drude model for the dc conductivity. Instead there is a very strong and broad background conductivity persisting throughout the infrared range. If the reciprocal relaxation time is 0.1 eV or larger, increasing with the frequency,[12] the interband structure will be significantly broadened. The inclusion of a broad dc term plus the contribution from other sources of relaxation may easily overshadow the interband term, which is then difficult to observe. Perhaps the strongest evidence for the existence of the interband conductivity as proposed in Fig. 10 is the recent measurement of the difference between σ^{yy} and σ^{xx}
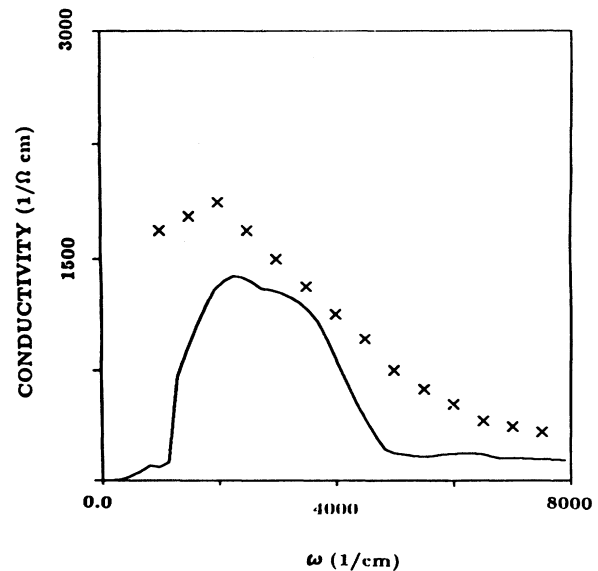

FIG. 10. Low-energy optical conductivity: solid line, σ^{xx}; long-dashed line, σ^{yy}; short-dashed line, σ^{zz}.

FIG. 11. A plot of calculated $\sigma^{yy} - \sigma^{xx}$ vs ω. Crosses are experimental data of Ref. 28.

reported by Schlesinger *et al.*[28] on single-domain (untwinned) crystals of $YBa_2Cu_3O_7$. In Fig. 11, we compare the calculated $\sigma^{yy} - \sigma^{xx}$ with the experimental data of Ref. 28. There is a good agreement between experiment and theory for the strength and position of the peak. It is also evident from Fig. 11 that the relaxation effects are very strong.

IV. SUMMARY

In this paper we have studied both real and imaginary parts of the dielectric function for $YBa_2Cu_3O_7$ as functions of the wave vector and the frequency. Our calculation is based on the random-phase approximation and we have used a set of tight-binding-band parameters based on the local-density functional LAPW bands. In addition to high-energy absorption peaks at 3.0 and 2.3 eV, we find very strong absorption peaks for energies below 0.5 eV. Our study shows these absorption peaks are associated with the rich Cu-O band structure adjacent to the Fermi level.

The presence of low-energy interband excitations as evidenced by large peaks in ϵ_2 is significant since they cause the existence of large regions of negatively valued ϵ_1 in the $\mathbf{q}, \omega$ space which may then lead to an effective attraction between electrons. It appears that the energy range in which the dielectric function is negative may be high and large enough in order to lead to a high T_c. However, in order to estimate T_c, band renormalization and contributions to ϵ from other kinds of elementary excitations must also be carefully considered. In addition, conventional procedures in which the $\mathbf{q}$ dependence of the effective interaction is averaged over directions will not be appropriate in this highly anisotropic case.

ACKNOWLEDGMENTS

APPENDIX

This appendix gives the general expression for the integrals defined in Eq. (2):

$$I \equiv \int U_i(\mathbf{r} - \mathbf{A})U_j(\mathbf{r} - \mathbf{B})\exp(i\mathbf{q}\cdot\mathbf{r})d\mathbf{r} , \qquad (A1)$$

where the two Gaussian functions are expressed as

$$U_i(\mathbf{r} - \mathbf{A}) = (x - A_x)^{l_1}(y - A_y)^{m_1}(z - A_z)^{n_1}$$
$$\times \exp[-\alpha_i(\mathbf{r} - \mathbf{A})^2] \qquad (A2)$$

and

$$U_j(\mathbf{r} - \mathbf{B}) = (x - B_x)^{l_2}(y - B_y)^{m_2}(z - B_z)^{n_2}$$
$$\times \exp[-\alpha_j(\mathbf{r} - \mathbf{B})^2] . \qquad (A3)$$

Defining $\alpha_p = \alpha_i + \alpha_j$ and $\mathbf{P} = (\alpha_i \mathbf{A} + \alpha_j \mathbf{B})/(\alpha_i + \alpha_j)$, it is easy to show

$$(x - A_x)^{l_1}(x - B_x)^{l_2}$$
$$= \sum_{n=0}^{l_1+l_2} d_x^{l_1,l_2}(n)\alpha_p^{n/2}H_n(\alpha_p(x - P_x)) , \qquad (A4)$$

where H_n is the Hermite polynomial and

$$d_x^{l_1,l_2}(n) = \frac{\alpha_p^{-n/2}}{n!} \sum_{i=0}^{l_1} \sum_{j=0}^{l_2} C_{l_1}^i C_{l_2}^j (P_x - A_x)^{(l_1-i)} ,$$
$$(P_x - B_x)^{(l_2-j)}\alpha_p^{-(i+j)/2}\frac{(i+j)!}{2^{i+j}[(i+j-n)/2]!} . \qquad (A5)$$

$C_{l_1}^i$ and $C_{l_2}^j$ are binomial functions. Using Eq. (A4), we can obtain the final result,

$$I = \exp\left[-\frac{\alpha_i\alpha_j}{\alpha_p}(\mathbf{A} - \mathbf{B})^2\right]\left[\frac{\pi}{\alpha_p}\right]^{3/2}\exp(-q^2/4\alpha_p)\exp(i\mathbf{q}\cdot\mathbf{P})$$
$$\times \sum_{r=0}^{l_1+l_2}\sum_{s=0}^{m_1+m_2}\sum_{t=0}^{n_1+n_2} d_x^{l_1,l_2}(r)d_y^{m_1,m_2}(s)d_z^{n_1,n_2}(t)(iq_x)^r(iq_y)^s(iq_z)^t . \qquad (A6)$$

[1] For a general review, see *High-Temperature Superconductivity*, edited by V. L. Ginzburg and D. A. Kirzhnit (Consultants Bureau, New York, 1982); see also P. B. Allen and B. Mitrovic, in *Solid State Physics*, edited by H. Ehrenreich, F. D. Seitz, and D. Turnbull (Academic, New York, 1982), Vol. 37, p. 1.

[2] M. J. DeWeert, D. A. Papaconstantopoulos, and W. E. Pickett, Phys. Rev. B **39**, 4235 (1989).

[3] H. Krakauer and W. E. Pickett, in *Novel Superconductivity*, edited by S. A. Wolf and V. Z. Kresin (Plenum, New York, 1987), p. 501.

[4] A. J. Arko, R. S. List, R. J. Bartlett, S. W. Cheong, Z. Fisk, J. D. Thompson, C. G. Olson, A. B. Yang, R. Liu, C. Gu, B. W. Veal, J. Z. Liu, A. P. Paulikas, K. Vandervoort, H. Claus, J. C. Campuzano, J. E. Schirber, and N. D. Shinn, Phys. Rev. B **40**, 2268 (1989).

[5] L. C. Smedskjaer, J. Z. Liu, R. Benedek, D. G. Legnini, D. J. Kim, M. D. Stahulak, H. Claus, and A. Bansil, Physica C **156**, 269 (1988).

[6] J. C. Campuzano, G. Jennings, M. Faiz, L. Beaulaigue, B. W. Veal, J. Z. Liu, A. P. Paulikas, K. Vandervoort, H. Claus, R. S. List, A. J. Arko, and R. J. Bartlett, Phys. Rev. Lett. **64**, 2308 (1990).

[7] C. Olson, Bull. Am. Phys. Soc. **35**, 407 (1990).

[8] See, for example, V. J. Emery, Phys. Rev. Lett. **58**, 2794 (1987); P. B. Anderson, Science **235**, 1196 (1987); J. R. Schrieffer, X.

G. Wen, and S. C. Zhang, Phys. Rev. Lett. **60**, 944 (1988).

[9]See, for example, N. W. Ashcroft, in *Novel Superconductivity* (Ref. 3), p. 301; C. M. Varma, S. Schmitt-Rink and E. Abrahams, *ibid.*, p. 355; D. L. Cox, M. Jarrell, C. Jayaprakash, H. R. Krishna-murthy, and J. Deisz, Phys. Rev. Lett. **62**, 2188 (1989).

[10]G. L. Zhao, Y. Xu, W. Y. Ching, and K. W. Wong, Phys. Rev. B **36**, 7203 (1987).

[11]S. T. Chui, R. V. Kasowski, and W. Y. Hsu, Phys. Rev. Lett. **61**, 885 (1988).

[12]Z. Schlesinger, R. T. Collins, F. Holtzberg, C. Feild, G. Koren, and A. Gupta, Phys. Rev. B **41**, 11 237 (1990).

[13]J. Yuan, L. M. Brown, and W. Y. Liang, J. Phys. C **21**, 517 (1988).

[14]C. H. Chen, L. F. Schneemeyer, S. H. Liou, M. Hong, J. Kwo, H. S. Chen, and J. V. Waszczak, Phys. Rev. B **37**, 9780 (1988).

[15]M. K. Kelly, Y. Meng, Y. Hwu, Y. Chang, Y. Chen, G. L. Capeyre, and G. Margaritondo, Phys. Rev. B **40**, 11 309 (1989).

[16]J. Callaway, *Quantum Theory of the Solid State* (Academic, New York, 1976), p. 584.

[17]D. A. Papaconstantopoulos (private communication).

[18]For Cu d: A. J. Wachters, J. Chem. Phys. **57**, 1033 (1971); for

O p: F. B. Duijneveldt, IBM Research Report No. RJ954, 1971 (unpublished).

[19]J. Rath and A. J. Freeman, Phys. Rev. B **11**, 2109 (1972).

[20]C. S. Wang and J. Callaway, Comp. Phys. Commun. **14**, 327 (1978).

[21]G. D. Mahan, *Many-Particle Physics* (Plenum, New York, 1981), p. 429.

[22]J. Callaway, *Quantum Theory of the Solid State* (Ref. 16), p. 517.

[23]E. Clementi and C. Roetti, At. Data Nucl. Data Tables **14**, 426 (1974) for Cu^+; **14**, 458 (1974) for O^-.

[24]J. Callaway, A. K. Chatterjee, S. P. Singhal, and A. Ziegler, Phys. Rev. B **28**, 3818 (1983).

[25]J. Hubbard, Proc. R. Soc. London, Ser. A **243**, 336 (1957).

[26]K. Kamaras, C. D. Porter, M. G. Doss, S. L. Herr, D. B. Tanner, D. A. Bonn, J. Z. Greedan, A. H. O'Reilly, C. V. Stager, and T. Timusk, Phys. Rev. Lett. **59**, 919 (1987).

[27]S. Tajima, H. Ishii, T. Nakahashi, T. Takagi, S. Uchida, M. Seki, S. Suga, Y. Hidaka, M. Suzuki, T. Murakami, K. Oka, and H. Unoki, J. Opt. Soc. Am. B **6**, 475 (1989).

[28]Z. Schlesinger, R. T. Collins, F. Holtzberg, C. Field, C. Blanton, U. Welp, G. W. Crabtree, Y. Fang, and J. Z. Liu, Phys. Rev. Lett. **65**, 801 (1990).